Proceedings of 20th International Congress on Acoustics, ICA 2010

23–27 August 2010, Sydney, Australia

Basic study on acoustic wave analysis by the multi-moment method using interpolation by a high-order polynomial

Masaki Tanigawa (1)

(1) SHIMIZU CORPORATION, the Institute of technology

PACS: 43.55.Ka

ABSTRACT

Many recent studies have used multi-moment methods such as the CIP (constrained interpolation profile) method for the analysis of acoustic wave propagation. The CIP method combines the method of characteristics and polynomial interpolation. This method has less numerical dispersion and is more stable than the FDTD (finite-difference time-domain) method. However, using the CIP method, numerical dissipation often causes a reduction in calculation accuracy. In order to reduce dissipation, we apply this method using interpolation by a fifth-order polynomial. However, as this scheme uses the physical values and their first- and second-order derivatives at the two nearest grid points, the computational load increases slightly. We propose a new algorithm to reduce memory requirements and examine the applicability of this scheme by computing wave propagations in two- and three-dimensional space. In this paper, we first derive the characteristic equations for acoustic waves using this scheme and then propose our new algorithm to reduce the memory requirement. Finally, we show some results of numerical simulations.

INTRODUCTION

The CIP ('cubic interpolated profile' or 'constrained interpolated profile') method, a multi-moment method [9, 8, 4], was proposed as a stable, low-dispersion algorithm developed for the field of CFD (computational fluid dynamics) and applied to many time-domain problems, including the analysis of acoustic wave propagation. In wave propagation analysis, the CIP method in combination with the method of characteristics (MOC) has been applied to simulate various wavefields and its applicability has been compared to that of other methods, such as the finite-difference time-domain (FDTD) method [3, 4, 7]. The FDTD method is commonly used in the field of architectural acoustics due to its simplicity and the ease with which it can be implemented in software. However, this method introduces numerical dispersion. The phase error of short-wavelength components is quite large, which distorts the waveforms as time progresses.

On the other hand, although the CIP method is low-dispersive, it causes numerical dissipation [1]. It is expected that this effect is especially large with certain wavefields for which simulations easily accumulate numerical errors, such as those describing rooms surrounded by rigid walls that generate many reflections. In order to obtain meaningful simulation results, it is necessary to reduce numerical dissipation.

In the CIP method, the wave profile is analyzed by interpolating by a cubic polynomial between two grid points at which the value of the wavefield and its first-order derivative are given. One way to reduce the dissipation is to interpolate using a high-order polynomial.

We adopt interpolation using a fifth-order polynomial instead of a cubic polynomial. In this scheme, the wave profile is evaluated between two neighboring points at which the values of the wavefield and its first- and second-derivatives are given. This scheme is compact because it only uses two points; however, there are many variables at each point, increasing the computational load.

In this paper, we apply this scheme using a fifth-order polynomial to simulate wave propagation by solving an acoustic wave equation and derive the characteristic equations of the wave. Then we propose an algorithm to reduce the memory requirements. Finally we show some results of numerical simulations for a simple rectangular model.

ANALYSIS

The phenomenon of the wave propagation in one-dimensional space obeys the following equations expressed in terms of pressure p and particle velocity u:

$$\frac{\partial p}{\partial t} + \rho c^2 \frac{\partial u}{\partial x} = 0, \tag{1}$$

$$\frac{\partial u}{\partial t} + \frac{1}{\rho}\frac{\partial p}{\partial x} = 0, \tag{2}$$

where ρ is the medium density, and c is the sound velocity. Eq. (1) is the equation of continuity, and Eq. (2) is the equation of motion in an acoustic medium.

From the above equations, we derive the two characteristic equations:

$$\frac{\partial f^+}{\partial t} + c\frac{\partial f^+}{\partial x} = 0, \tag{3}$$

$$\frac{\partial f^-}{\partial t} - c\frac{\partial f^-}{\partial x} = 0, \tag{4}$$

where $f^+ = p + \rho c u$ and $f^- = p - \rho c u$ are advection variables, and superscripts $+$ and $-$ indicate forward propagation ($c \geq 0$) and backward propagation ($c < 0$), respectively.

In the modeling of wave propagation based on MOC, Eqs. (3) and (4) are evaluated numerically using the CIP method.

Using this method, usually the wavefield between two grid points at which $f^{\pm}$ and their derivatives $f'^{\pm} = g^{\pm}$ are already known can be interpolated using a cubic polynomial. We will refer to this scheme using the notation CIP$_3$.

Interpolation by a fifth-order polynomial

In this paper, we interpolate by a fifth-order polynomial instead of a cubic polynomial.

As shown in Figure 1, let the advection variable $f(x)$ be defined on the interval $0 \le x \le L$. Define a uniform grid, $x_1 = 0 < x_2 < x_3 < \cdots < x_N < x_{N+1} = L$ with a spacing $\Delta x = x_{i+1} - x_i$. At any grid point x_i, assume that the advection valuable $f(x)$ and its derivatives $f_i' = g_i$, and $f_i'' = h_i$ are given.

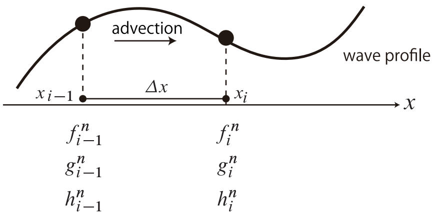

Figure 1: Symbols for adopting a fifth-order polynomial.

Let the wavefield between two neighboring points, x_i and $x_{i\,\mathrm{up}}$ ($i\,\mathrm{up} = i-1$ for the forward propagation, and $i\,\mathrm{up} = i+1$ for the backward propagation) be interpolated using a fifth-order polynomial,

$$F(x) = \sum_{k=1}^{6} a_k (x - x_i)^{k-1}. \tag{5}$$

The six coefficients $\{a_k,\ k = 1, 2, \ldots, 6\}$ in Eq. (5) are determined by the six equations:

$$\begin{aligned} &F(x_i) = f_i, \quad \frac{\partial F}{\partial x}(x_i) = g_i, \quad \frac{\partial^2 F}{\partial x^2}(x_i) = h_i, \\ &F(x_{i\,\mathrm{up}}) = f_{i\,\mathrm{up}}, \quad \frac{\partial F}{\partial x}(x_{i\,\mathrm{up}}) = g_{i\,\mathrm{up}}, \quad \frac{\partial^2 F}{\partial x^2}(x_{i\,\mathrm{up}}) = h_{i\,\mathrm{up}}. \end{aligned} \tag{6}$$

From above equations, the coefficients a_k are as follows:

$$\begin{aligned} a_1 &= -\frac{6(f_i - f_{i\,\mathrm{up}})}{D^5} - \frac{3(g_i + g_{i\,\mathrm{up}})}{D^4} - \frac{(h_i - h_{i\,\mathrm{up}})}{2D^3}, \\ a_2 &= \frac{15(f_i - f_{i\,\mathrm{up}})}{D^4} + \frac{8g_i + 7g_{i\,\mathrm{up}}}{D^3} + \frac{3h_i - 2h_{i\,\mathrm{up}}}{2D^2}, \\ a_3 &= -\frac{10(f_i - f_{i\,\mathrm{up}})}{D^3} - \frac{2(3g_i + 2g_{i\,\mathrm{up}})}{D^2} - \frac{3h_i - h_{i\,\mathrm{up}}}{2D}, \\ a_4 &= h_i/2, \quad a_5 = g_i, \quad a_6 = f_i, \end{aligned} \tag{7}$$

where $D = -\Delta x$ for the forward propagation, and $D = \Delta x$ for the backward propagation.

Let the advection variable at the n-th timestep be expressed by the superscript n. Then the profiles of f, g and h at the $(n+1)$-th timestep can be approximated by shifting the previous profiles using Eq. (5),

$$\begin{aligned} f_i^{n+1} &\simeq F(x_i - c\Delta t) \\ &= a_1\xi^5 + a_2\xi^4 + a_3\xi^3 + h_i^n/2\xi^2 + g_i^n\xi + f_i^n \end{aligned} \tag{8}$$

$$\begin{aligned} g_i^{n+1} &\simeq \frac{\partial F}{\partial x}(x_i - c\Delta t) \\ &= 5a_1\xi^4 + 4a_2\xi^3 + 3a_3\xi^2 + h_i^n\xi + g_i^n \end{aligned} \tag{9}$$

$$\begin{aligned} h_i^{n+1} &\simeq \frac{\partial^2 F}{\partial x^2}(x_i - c\Delta t) \\ &= 20a_1\xi^3 + 12a_2\xi^2 + 6a_3\xi + h_i^n, \end{aligned} \tag{10}$$

where Δt is the timestep and $\xi = -c\Delta t$.

We obtain the wavefield at the $(n+1)$-th timestep by linear summations of the forward and backward advection results:

$$\begin{aligned} p_i^{n+1} &= \frac{f_i^{n+1,+} + f_i^{n+1,-}}{2}, \quad & u_i^{n+1} &= \frac{f_i^{n+1,+} - f_i^{n+1,-}}{2\rho c}, \\ \partial_x p_i^{n+1} &= \frac{g_i^{n+1,+} + g_i^{n+1,-}}{2}, \quad & \partial_x u_i^{n+1} &= \frac{g_i^{n+1,+} - g_i^{n+1,-}}{2\rho c}, \\ \partial_{xx} p_i^{n+1} &= \frac{h_i^{n+1,+} + h_i^{n+1,-}}{2}, \quad & \partial_{xx} u_i^{n+1} &= \frac{h_i^{n+1,+} - h_i^{n+1,-}}{2\rho c}, \end{aligned} \tag{11}$$

where ∂_x and ∂_{xx} are defined as the spatial derivatives $\partial/\partial x$ and $\partial^2/\partial x^2$, respectively.

We will refer to the scheme described by Eqs. (5)–(11) by the notation CIP$_5$.

Applying CIP$_5$ to a multi-dimensional wavefield

In applying the CIP$_5$ scheme to multi-dimensional acoustic wave propagation, we adopt a direction splitting technique [5, 9].

In the three-dimensional case, first, we calculate the wavefields propagated in the x-direction, $\{p^*, u^{n+1}, \partial_x p^*, \partial_x u^{n+1}, \ldots\}$, from $\{p^n, u^n, \partial_x p^n, \partial_x u^n, \ldots\}$ and their derivatives using Eq. (11). Next, in the same way, we calculate the wavefields propagated in the y-direction, $\{p^{**}, v^{n+1}, \partial_y p^{**}, \partial_y v^n, \ldots\}$, from $\{p^*, v^n, \partial_y p^*, \partial_y v^n, \ldots\}$, and then calculate the wavefields propagated in the z-direction $\{p^{n+1}, w^{n+1}, \partial_z p^{n+1}, \partial_z w^n, \ldots\}$ from $\{p^{**}, w^n, \partial_z p^{**}, \partial_z w^n, \ldots\}$.

To use direction splitting, it is necessary to evaluate the propagations of the derivatives in the perpendicular directions. Table 1 shows the required calculations for the x-direction using the CIP$_5$ scheme and using the CIP$_3$ scheme. In Table 1, CIP$_5[f, g, h, x]$ indicates interpolation using f, $g = \partial x f$ and $h = \partial x x f$. Similarly, CIP$_3[f, g, x]$ indicates interpolation using f and g. Naturally, the same number of propagations must be evaluated in the y- and z-directions as in the x-direction.

Table 1: Required propagations in the x-direction to be evaluated using the CIP$_5$ and the CIP$_3$ schemes for a 2-D or a 3-D wavefield.

		CIP$_5$	CIP$_3$
3-D	2-D	CIP$_5[f, g, h, x]$ CIP$_5[\partial_y f, \partial_y g, \partial_y h, x]$ CIP$_5[\partial_{yy} f, \partial_{yy} g, \partial_{yy} h, x]$	CIP$_3[f, g, x]$ CIP$_3[\partial_y f, \partial_y g, x\ ]$
		CIP$_5[\partial_z f, \partial_z g, \partial_z h, x]$ CIP$_5[\partial_{zz} f, \partial_{zz} g, \partial_{zz} h, x]$ CIP$_5[\partial_{yz} f, \partial_{yz} g, \partial_{yz} h, x]$ CIP$_5[\partial_{yyz} f, \partial_{yyz} g, \partial_{yyz} h, x]$ CIP$_5[\partial_{yzz} f, \partial_{yzz} g, \partial_{yzz} h, x]$ CIP$_5[\partial_{yyzz} f, \partial_{yyzz} g, \partial_{yyzz} h, x]$	CIP$_3[\partial_z f, \partial_z g, x]$ CIP$_3[\partial_{yz} f, \partial_{yz} g, x]$

The CIP$_5$ scheme has more variables than the CIP$_3$ scheme. For two- and three-dimensional wavefields, the CIP$_5$ scheme has $(27 \times 2 \text{ timesteps} = 54)$ and $(108 \times 2 \text{ timesteps} = 216)$

variables at each grid point, respectively. Obviously, the computational load of the CIP_5 scheme is greater than the CIP_3 scheme.

In order to reduce the computational load of the CIP_5 scheme, the following new computation algorithm is proposed.

First, we express the combined form of forward and backward propagation from Eqs. (8)–(10) as the vector equation:

$$\begin{bmatrix} f_i^{n+1,\pm} \\ g_i^{n+1,\pm} \\ h_i^{n+1,\pm} \end{bmatrix} = \boldsymbol{M}^{\pm} \begin{bmatrix} f_i^{n,\pm} & g_i^{n,\pm} & h_i^{n,\pm} & f_{i\mathrm{up}}^{n,\pm} & g_{i\mathrm{up}}^{n,\pm} & h_{i\mathrm{up}}^{n,\pm} \end{bmatrix}^{\mathrm{T}}, \tag{12}$$

where

$$\boldsymbol{M}^{\pm} = \begin{bmatrix} \beta_1 & \pm\beta_2 & \beta_3 & \beta_{10} & \pm\beta_{11} & \beta_{12} \\ \pm\beta_4 & \beta_5 & \pm\beta_6 & \pm\beta_{13} & \beta_{14} & \pm\beta_{15} \\ \beta_7 & \pm\beta_8 & \beta_9 & \beta_{16} & \pm\beta_{17} & \beta_{18} \end{bmatrix}. \tag{13}$$

The 18 elements $\{\beta_m,\ m = 1,2,\ldots,18\}$ in Eq. (13) are given by

$$\begin{aligned}
\beta_1 &= (\delta-\xi)^3)(\delta^2+3\delta\xi+6\xi^2)/\delta^5, \\
\beta_2 &= (\delta-\xi)^3)(\delta^2+3\delta\xi)/\delta^4, \\
\beta_3 &= \xi^2(\delta-\xi)^3/(2\delta^3), \\
\beta_4 &= -30\xi^2(\delta-\xi)^2/\delta^5, \\
\beta_5 &= (\delta-3\xi)(\delta-\xi)^2(\delta+5\xi)/\delta^4, \\
\beta_6 &= \xi(\delta-\xi)^2(2\delta-5\xi)/(2\delta^3), \\
\beta_7 &= -60\xi(\delta-2\xi)(\delta-\xi)/\delta^5, \\
\beta_8 &= -12\xi(3\delta-5\xi)(\delta-\xi)/\delta^4, \\
\beta_9 &= (\delta-\xi)(\delta^2-8\delta\xi+10\xi^2)/\delta^3, \\
\beta_{10} &= \xi^3(10\delta^2-15\delta\xi+6\xi^2)/\delta^5, \\
\beta_{11} &= -\xi^3(4\delta-3\xi)(\delta-\xi)/\delta^4, \\
\beta_{12} &= \xi^3(\delta-\xi)^2/(2\delta^3), \\
\beta_{13} &= 30\xi^2(\delta-\xi)^2/\delta^5, \\
\beta_{14} &= -\xi^2(6\delta-\xi)(2\delta-3\xi)/\delta^4, \\
\beta_{15} &= \xi^2(3\delta-5\xi)(\delta-\xi)/(2\delta^3), \\
\beta_{16} &= 60\xi(\delta-\xi)(\delta-\xi)/\delta^5, \\
\beta_{17} &= -12\xi(2\delta-5\xi)(\delta-\xi)/\delta^4, \\
\beta_{18} &= \xi(3\delta^3-12\delta\xi+10\xi^2)/(2\delta^3),
\end{aligned} \tag{14}$$

where $\delta = |c|\Delta t$.

Let the matrix $\boldsymbol{Q}^n$ consist of the variables involved in one advection calculation using the CIP_5 scheme. In the case of $\mathrm{CIP}_5[f,g,h,x]$, $\boldsymbol{Q}^n$ is given by

$$\boldsymbol{Q}^n = \begin{bmatrix} \boldsymbol{p}^n & \boldsymbol{u}^n & \partial_x\boldsymbol{p}^n & \partial_x\boldsymbol{u}^n & \partial_{xx}\boldsymbol{p}^n & \partial_{xx}\boldsymbol{u}^n \end{bmatrix}, \tag{15}$$

where $\boldsymbol{p}^n$, $\boldsymbol{u}^n$, $\partial_x\boldsymbol{p}^n$, $\partial_x\boldsymbol{u}^n$, $\partial_{xx}\boldsymbol{p}^n$ and $\partial_{xx}\boldsymbol{p}^n$ are the column-vectors,

$$\boldsymbol{p}^n = (p_1^n, p_2^n, \ldots, p_M^n, p_{M+1}^n)^{\mathrm{T}}, \tag{16}$$

$$\boldsymbol{u}^n = (u_1^n, u_2^n, \ldots, u_M^n, u_{M+1}^n)^{\mathrm{T}}, \tag{17}$$

$$\partial_x\boldsymbol{p}^n = (\partial_x p_1^n, \partial_x p_2^n, \ldots, \partial_x p_M^n, \partial_x p_{M+1}^n)^{\mathrm{T}}, \tag{18}$$

$$\partial_x\boldsymbol{u}^n = (\partial_x u_1^n, \partial_x u_2^n, \ldots, \partial_x u_M^n, \partial_x u_{M+1}^n)^{\mathrm{T}}, \tag{19}$$

$$\partial_{xx}\boldsymbol{p}^n = (\partial_{xx} p_1^n, \partial_{xx} p_2^n, \ldots, \partial_{xx} p_M^n, \partial_{xx} p_{M+1}^n)^{\mathrm{T}}, \tag{20}$$

$$\partial_{xx}\boldsymbol{u}^n = (\partial_{xx} u_1^n, \partial_{xx} u_2^n, \ldots, \partial_{xx} u_M^n, \partial_{xx} u_{M+1}^n)^{\mathrm{T}}. \tag{21}$$

Then, we perform the following six matrix multiplications:

$$\begin{aligned}
\boldsymbol{Q}^n\boldsymbol{F}_{\mathrm{add}} &= [a_{ij}], & \boldsymbol{Q}^n\boldsymbol{F}_{\mathrm{sub}} &= [\hat{a}_{ij}], \\
\boldsymbol{Q}^n\boldsymbol{G}_{\mathrm{add}} &= [b_{ij}], & \boldsymbol{Q}^n\boldsymbol{G}_{\mathrm{sub}} &= [\hat{b}_{ij}], \\
\boldsymbol{Q}^n\boldsymbol{H}_{\mathrm{add}} &= [c_{ij}], & \boldsymbol{Q}^n\boldsymbol{H}_{\mathrm{sub}} &= [\hat{c}_{ij}].
\end{aligned} \tag{22}$$

The six matrices $\boldsymbol{F}_{\mathrm{add}}$, $\boldsymbol{F}_{\mathrm{sub}}$, $\boldsymbol{G}_{\mathrm{add}}$, $\boldsymbol{G}_{\mathrm{sub}}$, $\boldsymbol{H}_{\mathrm{add}}$ and $\boldsymbol{H}_{\mathrm{sub}}$ in Eqs. (22) are given by

$$\boldsymbol{F}_{\mathrm{add}} = \frac{1}{2}\begin{bmatrix} \beta_{10} & 2\beta_1 & \beta_{10} \\ \rho c\beta_{10} & 0 & -\rho c\beta_{10} \\ -\beta_{11} & 0 & \beta_{11} \\ -\rho c\beta_{11} & -2\rho c\beta_2 & -\rho c\beta_{11} \\ \beta_{12} & 2\beta_3 & \beta_{12} \\ \rho c\beta_{12} & 0 & -\rho c\beta_{12} \end{bmatrix} \tag{23}$$

$$\boldsymbol{F}_{\mathrm{sub}} = \frac{1}{2\rho c}\begin{bmatrix} \beta_{10} & 0 & -\beta_{10} \\ \rho c\beta_{10} & 2\rho c\beta_1 & \rho c\beta_{10} \\ -\beta_{11} & -2\beta_2 & -\beta_{11} \\ -\rho c\beta_{11} & 0 & \rho c\beta_{11} \\ \beta_{12} & 0 & -\beta_{12} \\ \rho c\beta_{12} & 2\beta_3 & \rho c\beta_{12} \end{bmatrix} \tag{24}$$

$$\boldsymbol{G}_{\mathrm{add}} = \frac{1}{2}\begin{bmatrix} -\beta_{13} & 0 & \beta_{13} \\ -\rho c\beta_{13} & -2\rho c\beta_4 & -\rho c\beta_{13} \\ \beta_{14} & 2\beta_5 & \beta_{14} \\ \rho c\beta_{14} & 0 & -\rho c\beta_{14} \\ -\beta_{15} & 0 & \beta_{15} \\ -\rho c\beta_{15} & -2\rho c\beta_6 & -\rho c\beta_{15} \end{bmatrix} \tag{25}$$

$$\boldsymbol{G}_{\mathrm{sub}} = \frac{1}{2\rho c}\begin{bmatrix} -\beta_{13} & -2\beta_4 & -\beta_{13} \\ -\rho c\beta_{13} & 0 & \rho c\beta_{13} \\ \beta_{14} & 0 & -\beta_{14} \\ \rho c\beta_{14} & 2\rho c\beta_5 & \beta_{14} \\ -\beta_{15} & -2\beta_6 & -\beta_{15} \\ -\rho c\beta_{15} & 0 & \rho c\beta_{15} \end{bmatrix} \tag{26}$$

$$\boldsymbol{H}_{\mathrm{add}} = \frac{1}{2}\begin{bmatrix} \beta_{16} & 2\beta_7 & \beta_{16} \\ \rho c\beta_{16} & 0 & -\rho c\beta_{16} \\ -\beta_{17} & 0 & \beta_{17} \\ -\rho c\beta_{17} & -2\rho c\beta_8 & -\rho c\beta_{17} \\ \beta_{18} & 2\beta_9 & \beta_{18} \\ \rho c\beta_{18} & 0 & -\rho c\beta_{18} \end{bmatrix} \tag{27}$$

$$\boldsymbol{H}_{\mathrm{sub}} = \frac{1}{2\rho c}\begin{bmatrix} \beta_{16} & 0 & -\beta_{16} \\ \rho c\beta_{16} & 2\rho c\beta_7 & \rho c\beta_{16} \\ -\beta_{17} & -2\beta_8 & -\beta_{17} \\ -\rho c\beta_{17} & 0 & \rho c\beta_{17} \\ \beta_{18} & 0 & -\beta_{18} \\ \rho c\beta_{18} & 2\rho c\beta_9 & \rho c\beta_{18} \end{bmatrix}. \tag{28}$$

As shown in Figure 2, p_i, u_i and their derivatives $(i = 2,3,,\ldots,M-1,M)$ at the $n+1$-th step can each be expressed as the sum of three terms:

$$\begin{aligned}
p_i^{n+1} &= a_{i-1,1} + a_{i,2} + a_{i+1,3}, \\
u_i^{n+1} &= \hat{a}_{i-1,1} + \hat{a}_{i,2} + \hat{a}_{i+1,3}, \\
\partial_x p_i^{n+1} &= b_{i-1,1} + b_{i,2} + b_{i+1,3}, \\
\partial_x u_i^{n+1} &= \hat{b}_{i-1,1} + \hat{b}_{i,2} + \hat{b}_{i+1,3}, \\
\partial_{xx} p_i^{n+1} &= c_{i-1,1} + c_{i,2} + c_{i+1,3}, \\
\partial_{xx} u_i^{n+1} &= \hat{c}_{i-1,1} + \hat{c}_{i,2} + \hat{c}_{i+1,3}.
\end{aligned} \tag{29}$$

$$\boldsymbol{Q}^n \boldsymbol{F}_{\text{add}} = [a_{ij}] =$$

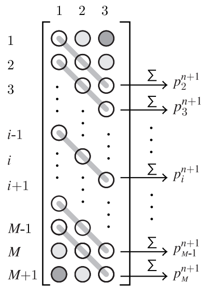

Figure 2: Representing physical variables (Eq. (29))

Boundary conditions

At x_1 and x_{M+1}, the physical variables and their derivatives can not be obtained directly from Eqs. (29). Instead, these variables are determined by using a boundary condition formula. However, in many cases, this is a relatively straightforward calculation.

For the case $i=1$, if $\dot{p}_1 = (a_{2,2}+a_{3,3})$ and $\dot{u}_1 = (\hat{a}_{2,2}+\hat{a}_{3,3})$, then clearly $\dot{p}_1 - \rho c \dot{u}_1$ is equal to the backward propagation $f_1^{n+1,-}$. Similarly, $\dot{p}_{M+1} + \rho c \dot{u}_{M+1}$ is equal to the forward propagation $f_{M+1}^{n+1,+}$.

For example, if the boundary at x_1 is non-reflecting, as shown in Figure 3, the forward propagation is zero. Therefore, from Eqs. (11), p_1^{n+1} and u_1^{n+1} are given by

$$\begin{aligned} p_1^{n+1} &= f_1^{n+1,-}/2 = (\dot{p}_1 - \rho c \dot{u}_1)/2, \\ u_1^{n+1} &= -f_1^{n+1,-}/(2\rho c) = -(\dot{p}_1 - \rho c \dot{u}_1)/(2\rho c). \end{aligned} \tag{30}$$

The derivatives of p_1^{n+1} and u_1^{n+1} are obtained similarly.

Many other boundary conditions (i.e., periodic, reflecting boundaries) can be handled easily in a similar manner.

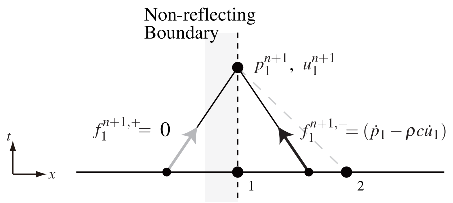

Figure 3: Example of computing boundary variables (non-reflecting).

Coding

The six matrix multiplications in Eqs. (22) are all of the same form and can be evaluated sequentially. Moreover, using these multiplications and evaluating the boundary conditions, it is easy to re-construct the forward or backward advection variables from the results of the matrix multiplications.

Therefore, it is not necessary to maintain in memory the values of variables at two time-steps (n and $n+1$); if a working array of the size of $\boldsymbol{Q}^n$ in Eqs. (15) is prepared, this scheme requires memory for one time-step only.

First, let $\boldsymbol{Q}$ at the n-th timestep consist of the variables used for the CIP$_5$ scheme in Eq. (15) and let $\boldsymbol{Q}$ be copied to the work array. Then, the results evaluated by the CIP$_5$ scheme at the $n+1$-th timestep in Eqs. (29) overwrite $\boldsymbol{Q}$ (that is, $\boldsymbol{Q}$ is updated). Other propagations in Table 1 are computed similarly.

In addition, Eqs. (22) assumes $\boldsymbol{Q}^n$ is the matrix in column-major order (the columns are listed in sequence in liner memory).

RESULTS

Numerical stability

Figure 4 shows the numerical stabilities of the CIP$_5$ and CIP$_3$ schemes using the von Neumann method in the one-dimensional case. The stabilities of the up-wind (1st), the Lax-Wendrof and the FTCS (2nd) schemes are also illustrated. Let CFL $= (|c|\Delta t/\Delta x)$ be the CFL (Courant-Friedrichs-Lewy) number. It has been proved analytically and numerically that the CIP scheme is stable [2, 6] for $0 \le \text{CFL} \le 1$. As shown in Figure 4, the CIP$_5$ scheme has lower attenuation of the amplitude than the CIP$_3$ scheme for high frequencies.

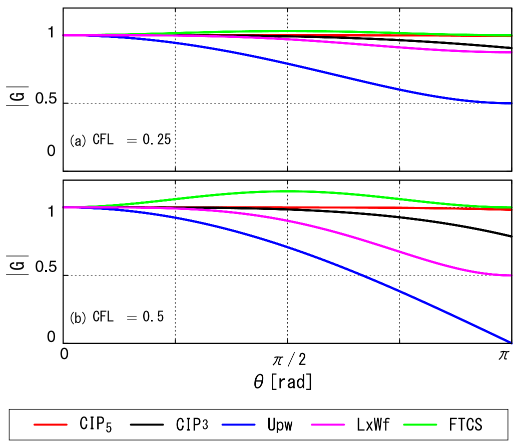

Figure 4: Comparison of numerical stabilities of CIP$_5$, CIP$_3$, 1st up-wind (`Upw`), Lax-Wendrof (`LxWf`) and 2nd FTCS schemes by using the von Neumann method. G is the amplification factor and θ is the phase angle. (a) CFL $= 0.25$, (b) CFL $= 0.5$.

Multi-dimensional wavefields

Figure 5 shows a rectangular area ($L_x \times L_y = 8$ m $\times$ 8 m) for a numerical simulation in two-dimensional space. The grid spacing is $\Delta x = \Delta 0.04$ m, defining an 200×200 grid. There is a sound source at the center of the area, $\boldsymbol{r}_0 = (0,0)$. The initial pressure ($t=0$) is given by the spatial gauss function,

$$p_0(\boldsymbol{r}) = e^{-r^2/d_0^2}, \quad r = |\boldsymbol{r} - \boldsymbol{r}_0|, \tag{31}$$

where d_0 determines the width of the spatial Gauss function, which here is defined as $d_0 = \sqrt{2}\pi f_0/c$. The frequency f_0 refers to the peak frequency in the spectrum of the wave expressed in Eq. (31).

We calculate the wave propagations in this numerical model using the CIP$_5$ scheme and using the CIP$_3$ scheme. We use two types of CIP$_3$ scheme, Type-C and Type-M. The Type-M scheme uses a first-order up-wind scheme to calculate derivatives in the perpendicular direction. This method has lower accuracy; however, it has the advantage of using less memory.

Figure 6 shows the sound pressure calculated using each method at the receiving point $\boldsymbol{r} = (L_x/4, L_y/4)$. The parameters values used are CFL $= 0.25,\ 0.5$ and $f_0 = 230,\ 460$ Hz.

In the case of CFL $= 1$, interpolation by a polynomial is unnecessary for evaluating wave propagation. In order to examine the interpolation accuracy of each scheme, we use the results of the case CFL $= 1$ as a reference.

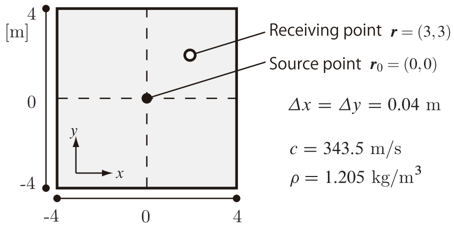

Figure 5: Rectangular wavefield in 2-D space.

As shown in Figure 6, for the case $f_0 = 230$ Hz, all the methods are fairly accurate. On the other hand, for the case $f_0 = 680$ Hz, the accuracies of the Type-C and the Type-M scheme worsen while the CIP$_5$ scheme remains relatively accurate.

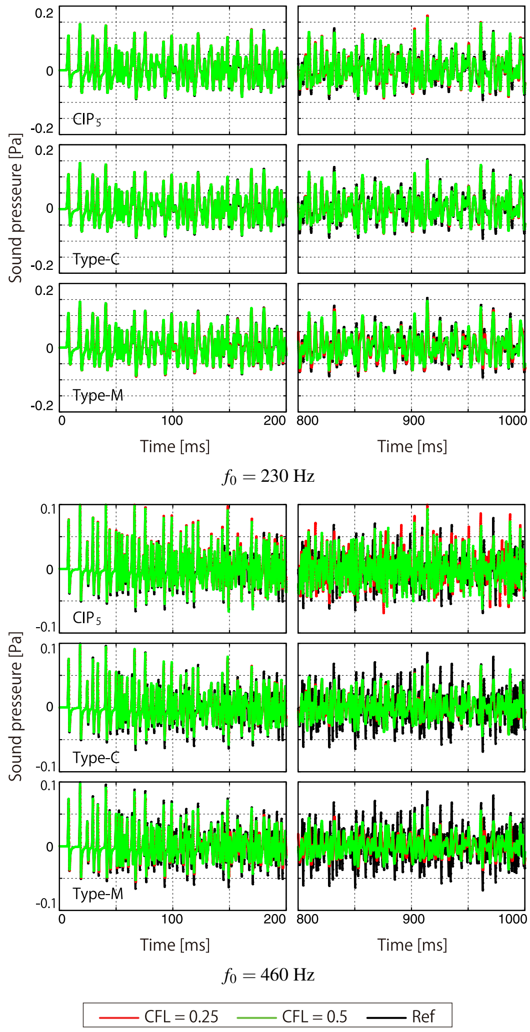

Figure 6: Numerical results in a 2-D rectangular area using CIP$_5$, Type-C and Type-M for $f_0 = 230$ Hz and 460 Hz.

Figure 7 shows the moving averages (100 ms intervals) of the sound pressure level (SPL) at the receiving point $\boldsymbol{r}$. As shown in Figure 7, when the source signal contains only relatively low frequencies ($f_0 = 230$ Hz), all methods are fairly accurate. However, when the source signal includes high-frequency components, the accuracies of the Type-C and Type-M methods get worse over time. For the case $f_0 = 680$ Hz, the accuracies of Type-C and Type-M are reduced by about 3 to 5 dB at $t = 5000$ ms and about 6 to 8 dB at $t = 1000$ ms relative to the reference (CFL $= 1$). On the other hand, the CIP$_5$ method stays relatively accurate.

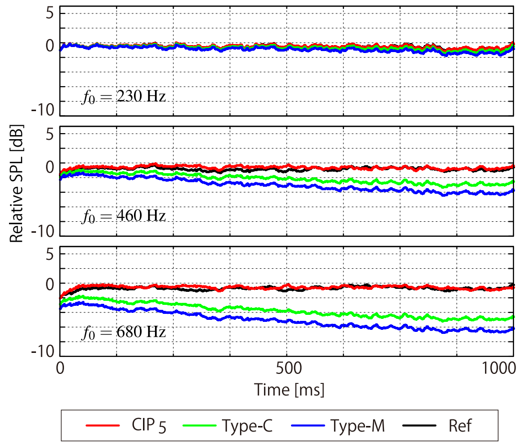

Figure 7: Comparison of moving average of sound pressure level for $f_0 = 230$ Hz, 460 Hz and 680 Hz.

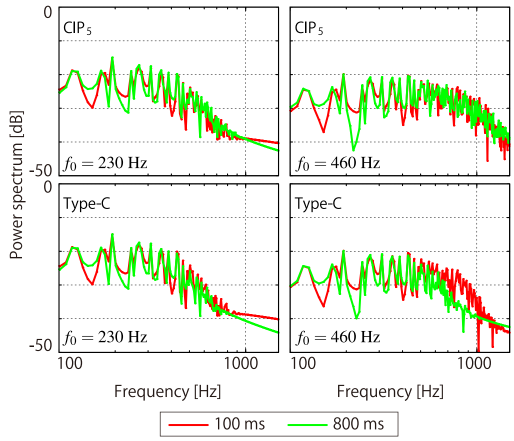

Figure 8: Comparison of power spectrum at $t = 100$ ms and 1000 ms: The FFT length is 2048 points.

Figure 8 shows the power spectrum at $t = 500$ ms and $t = 1000$ ms. As shown in Figure 8, the spectrums of both the Type-C and the Type-M schemes are maintained relatively well for low frequencies, but degrade for high frequencies. On the other hand, the CIP$_5$ method has an accuracy that does not get worse, independent of the frequencies.

In order to evaluate the error of each method, the following formula is defined:

$$error = \sum_{n=1}^{N} \{p^n(\boldsymbol{r}) - p^n_{\mathrm{ref}}(\boldsymbol{r})\}^2 \Big/ \sum_{n=1}^{N} \{p^n_{\mathrm{ref}}(\boldsymbol{r})\}^2 \qquad (32)$$

where N is the interval steps, $p^n(\boldsymbol{r})$ is the pressure and $p^n_{\mathrm{ref}}(\boldsymbol{r})$ is the pressure for the case $CFL = 1$ (non-interpolated) at the receiving point $\boldsymbol{r}$, respectively.

Table 2 shows the results of the error analyses at $t = 0$, 200, 400 and 600 ms using Eq. (32). The interval is 200 ms. Early ($t = 0$ ms), the errors of all the methods are relatively small. As time progresses, the error grows larger. Especially, Type-C and Type-M methods tend to have larger errors at high frequencies and at large CFL numbers. This is the result of numerical errors accumulating in the wavefield when many reflected waves are involved.

Similar trends appears in the three-dimensional case as the two-dimensional case. Figure 9 shows a rectangular box with rigid

Table 2: Result of error analysis using Eq. (32).

$f_0 = 230$ Hz, CFL $= 0.5$

Interval	CIP$_5$	Type-C	Type-M
0–200 ms	1.48×10^{-3}	1.69×10^{-3}	2.34×10^{-3}
200–400 ms	1.09×10^{-3}	2.57×10^{-3}	6.50×10^{-3}
400–600 ms	2.05×10^{-3}	5.56×10^{-3}	1.36×10^{-2}
600–800 ms	4.22×10^{-3}	1.08×10^{-2}	2.35×10^{-2}

$f_0 = 230$ Hz, CFL $= 0.25$

Interval	CIP$_5$	Type-C	Type-M
0–200 ms	5.58×10^{-10}	5.99×10^{-4}	7.99×10^{-3}
200–400 ms	4.23×10^{-9}	3.61×10^{-3}	4.45×10^{-2}
400–600 ms	1.21×10^{-8}	8.13×10^{-3}	9.33×10^{-2}
600–800 ms	2.36×10^{-8}	1.47×10^{-2}	1.45×10^{-1}

$f_0 = 460$ Hz, CFL $= 0.5$

Interval	CIP$_5$	Type-C	Type-M
0–200 ms	8.19×10^{-3}	3.09×10^{-2}	6.31×10^{-2}
200–400 ms	4.69×10^{-2}	1.00×10^{-1}	1.67×10^{-1}
400–600 ms	1.11×10^{-1}	1.79×10^{-1}	2.57×10^{-1}
600–800 ms	1.85×10^{-1}	2.36×10^{-1}	3.01×10^{-1}

$f_0 = 460$ Hz, CFL $= 0.25$

Interval	CIP$_5$	Type-C	Type-M
0–200 ms	2.92×10^{-6}	4.42×10^{-2}	1.55×10^{-1}
200–400 ms	1.27×10^{-5}	1.27×10^{-1}	0.39×10^{-1}
400–600 ms	3.49×10^{-5}	2.02×10^{-1}	5.21×10^{-1}
600–800 ms	6.00×10^{-5}	2.44×10^{-1}	5.84×10^{-1}

walls (5 m $\times$ 7 m $\times$ 3 m) in the three-dimensional space. There is a sound source at the center of the box, $\boldsymbol{r}_0 = (0,0,0)$. The grid spacing is $\Delta x = \Delta 0.04$ m, defining an $125 \times 175 \times 75$ grid.

Figure 10 shows the contour maps resulting from calculating sound pressure in xy-plane. As shown in Figure 10, the CIP$_5$ scheme maintains a lower level of dissipation than the Type-C scheme, even as time passes.

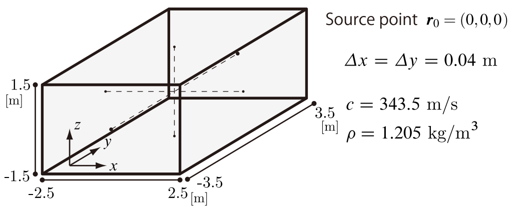

Figure 9: Rectangular wavefield in 3-D space.

CONCLUSIONS

The CIP$_5$ scheme using interpolation by a fifth-order polynomial has lower dissipation than the CIP$_3$ scheme, especially at high frequencies. Moreover, collapse over time of the waveforms is reduced by using this scheme. Although the computational load of the CIP$_5$ scheme is higher than the CIP$_3$ scheme, the memory requirements can be substantially reduced by making improvements to the algorithm.

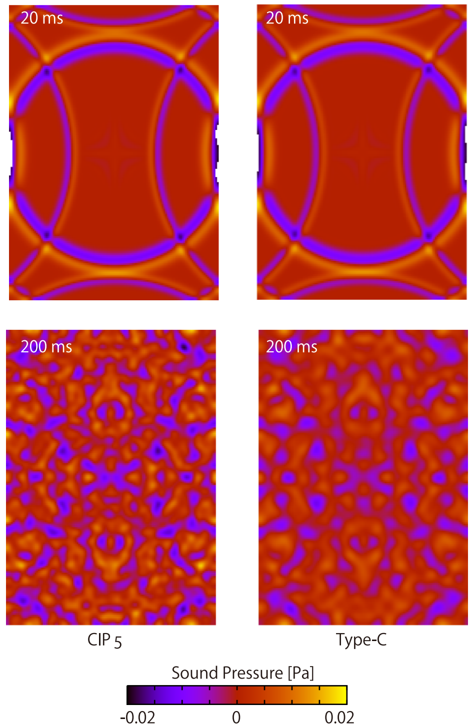

Figure 10: Contour maps of sound pressure in the xy-plane calculated using the CIP$_5$ and Type-C methods.

REFERENCES

[1] M. Konno et al. "Performances of Various Types of Constrained Interpolation Profile Method for Two-Dimensional Numerical Acoustic Simulation (Communication)". *Japanese Journal of Applied Physics-Part 1 Regular Papers and Short Notes* 47.5 (2008), pp. 3962–3963.

[2] M. Nara and R. Takaki. "Stability Analysis of the CIP Scheme." *Transactions of the Institute of Electronics, Information and Communication Engineers. A* J85–A.9 (2002), pp. 950–953.

[3] H. OKUBO and N. TAKEUCHI. "Numerical Analysis of Electromagnetic Field Generated by Line Current Using the CIP Method". *IEIC Technical Report (Institute of Electronics, Information and Communication Engineers)* 104.677 (2005), pp. 197–202.

[4] K. Shiraishi and T. Matsuoka. "Wave Propagation Simulation Using the CIP Method of Characteristic Equations". *Communications in Computational Physics* 3.1 (2008), pp. 121–135.

[5] H. Takewaki and T. Yabe. "The cubic-interpolated Pseudo particle (cip) method: application to nonlinear and multi-dimensional hyperbolic equations". *Journal of Computational Physics* 70.2 (1987), pp. 355–372.

[6] T. Utsumi, T. Kunugi, and T. Aoki. "Stability and accuracy of the cubic interpolated propagation scheme". *Computer Physics Communications* 101.1-2 (1997), pp. 9–20.

[7] S. Watanabe, Y. Kakuta, and O. Hashimoto. "Analytical study of rectangle wave propagation in electromangetic field using FDTD, CIP, and R-CIP methods". *Microwave and Optical Technology Letters* 48.10 (2006), pp. 1940–1943.

[8] T. Yabe, F. Xiao, and T. Utsumi. "The constrained interpolation profile method for multiphase analysis". *Journal of Computational Physics* 169.2 (2001), pp. 556–593.

[9] T. Yabe et al. "A universal solver for hyperbolic equations by cubic-polynomial interpolation I. One-dimensional solver". *Computer Physics Communications* 66.2-3 (1991), pp. 219–232.